EDUCATUM JSMT Vol. 6 No. 1 (2019)
ISSN 2289-7070 / eISSN 2462-2451 (35-40)
http://ojs.upsi.edu.my/index.php/EJSMT/index

Extrema Points Application in Determining Iris Region of Interest

Zuraini Othman[1*], Azizi Abdullah[2], Sharifah Sakinah Syed Ahmad[1]and Fauziah Kasmin[1]

[1]Department of Intelligent Computing and Analytics, Faculty of information & Communication Technology, Universiti Teknikal Malaysia Melaka, 76100 Hang Tuah Jaya Melaka, Malaysia.
[2]Center for Artificial Intelligence Technology, Faculty of information Science and Technology, Universiti Kebangsaan Malaysia 43600 Bangi, Selangor Darul Ehsan, Malaysia.

**Corresponding auothor: zuraini*@utem.edu.my

Received: 13 May 2019; Accepted: 06 June 2019; Published: 26 June 2019

Abstract

Extrema points are usually applied to solve everyday problems, for example, to determine the potential of a created tool and for optimisation. In this study, extrema points were used to help determine the region of interest (ROI) for the iris in iris recognition systems. Iris recognition is an automated method of biometric identification that uses mathematical pattern-recognition techniques on the images of one or both irises of an individual's eyes, where the complex patterns are unique, stable, and can be seen from a distance. In order to obtain accurate results, the iris must be localised correctly. Hence, to address this issue, this paper proposed a method of iris localisation in the case of ideal and non-ideal iris images. In this study, the algorithm was based on finding the classification for the region of interest (ROI) with the help of a Support Vector Machine (SVM) by applying a histogram of grey level values as a descriptor in each region from the region growing technique. The valid ROI was found from the probabilities graph of the SVM obtained by looking at the global minimum conditions determined by a second derivative model in a graph of functions. Furthermore, the model from the global minimum condition values was used in the test phase, and the results showed that the ROI image obtained helped in the elimination of sensitive noise with the involvement of fewer computations, while reserving relevant information.

Keywords Extrema Points; Region of Interest (ROI); Region Growing; Iris Recognition System.

INTRODUCTION

Extrema points are involved in many applications, not only for determining the rate of change. In computer vision, for example, in handwritten verifications, the shape of the extrema points are used to identify the shape of a signature[1][2]. Other than that, video and image processing also apply extrema points by using a bi-dimensional empirical mode [3][4][5] for standard images, video and hyperspectral images. In this paper, extrema points helped to determine the region of interest (ROI) in an image of the iris. The features of the iris are considered as one of the most reliable biometrics. Thus, they play an important role in the correct identification of humans as every individual has a unique pair of eyes, which is true even of twins, and the eye data is stable over time [6][7].

Iris recognition systems are widely used in the biometric and iris diagnosis fields. The iris biometric system was designed to help in the process of the identification of persons [8]. In iris diagnosis, the surface of the iris is divided into a specific number of segments, with each segment being related to an organ, apparatus or system [9]. As a result, several iris recognition systems have been built using different processes but with a similar objective of producing improved iris images for many applications in iris diagnosis and biometrics. Generally, an iris recognition system consists of three main building blocks, i.e., iris image acquisition, detection of iris life and recognition [10]. The accuracy of the iris recognition system is dependent on the accuracy of the iris localisation and classification. If this stage fails, the person will not be properly recognised [11].

Iris localisation determines the inner and the outer iris boundaries, thereby indicating the upper and the lower bounds of the eyelids. The inner circle represents the area between the boundary of the pupil and the iris, whereas the outer circle represents the area between the boundary of the iris and the sclera (see Figure 1).

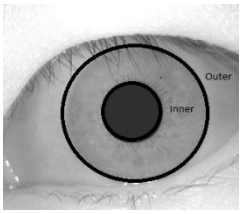

FIG. 1 Iris Boundaries

In this study, a suitable algorithm was proposed for the ideal and non-ideal iris images instead of the algorithm being merely suitable for ideal iris images as in [12]. Here, region growing with supervised learning using the SVM was used to obtain robustness and to increase the accuracy of the iris localisation. Information regarding the intensity of the grey level histogram was gathered in the training phase. Next, the pattern of the probabilities obtained from the SVM in each region (R) from the region growing gave valuable information on the ROI classification with support from the mathematical theory in the created graph. The dataset from the CASIA V2 was used for the ideal iris images and from the UBIRIS2 for the non-ideal iris images in this study. Lastly, the adaptive method from [13] was used to determine whether the proposed technique was able to localise the actual iris boundaries.

MATERIALS AND METHOD

Region growing

In this study, a merging region growing was used. The region was segmented from the circle of the pupil and it was completed until the end of the eye image. It was represented as R (see Figure 2).

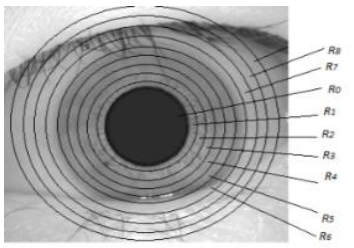

FIG. 2 Region growing in eye image

Global minimum with second derivatives and SVM

The function was represented as $Pb(R)$ because the values of the function were the probabilities (Pb) that would be plotted to the respective values of R . [14][15] discussed the occurrence of the local maximum and local minimum or saddle point, when the value of the gradient is

$$Pb'(R) = 0\,, \tag{1}$$

where the gradient is zero at the top and bottom of the graph, and the point R is known as the critical point. In order to solve $Pb'(R)$ in Equation (1), let point A be $(R_i, Pb(R_i))$ and point B be $(R_{i+1}, Pb(R_{i+1}))$ in function

$Pb(R)$, so that the gradient is : $Pb'(R) = \dfrac{dPb(R)}{dR} \cong \dfrac{\Delta Pb(R)}{\Delta R} = \dfrac{Pb(R_{i+1}) - Pb(R_i)}{R_{i+1} - R_i}$ (2)

From all the information, the first order derivative, which is Equation (2), was created from the Taylor Series to become

$$Pb(R_{i+1}) \cong \frac{Pb(R_{i+1}) - Pb(R_i)}{R_{i+1} - R_i} = \frac{Pb(R_{i+1}) - Pb(R_i)}{h} \tag{3}$$

Hence, the second derivative was

$$Pb''(R) \cong \frac{\left(\frac{Pb(R_{i+1}) - Pb(R_i)}{h}\right) - \left(\frac{Pb(R_i) - Pb(R_{i-1})}{h}\right)}{h} \tag{4}$$

In Equation (4), the more accurately-centred difference was used to become

$$Pb''(R) \cong \frac{Pb(R_{i+1}) - 2Pb(R_i) + Pb(R_{i-1})}{h^2} \tag{5}$$

Similar patterns were found from the graph of the SVM probability value (*Pb*) in the training and validating phase. The value of $h = 1$ was used as it represented $R_0, R_1, R_2, ..., R_n$. So, Equation (4) became

$$Pb''(R_i) \cong Pb(R_{i+1}) - 2Pb(R_i) + Pb(R_{i-1}) \tag{6}$$

The localised iris was found at the minimum point of the graph. As illustrated in Figure 3, the ROI of the iris was in the radius of R_{15}.

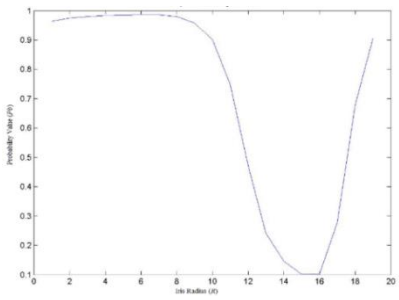

FIG. 3 Graph of SVM probability

The graph in Figure 3 represents the probabilities in each region in the region growing, which were plotted in the graph, as shown in Figure 4. This demonstrated that the *Pb* value decreased until it was near to the ROI image, then, it increased when it was beyond the ROI.

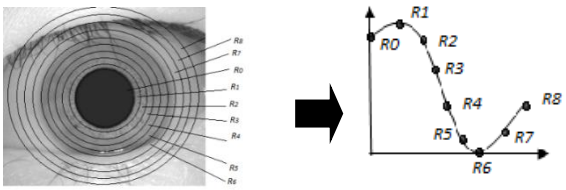

FIG. 4 Graph of SVM probability

In the testing phase, the algorithm was terminated once the critical point from the value of $(R_i, Pb(R_i))$ satisfied the $Pb''(R_i) > 0$ condition. Hence, to ensure that $(R_i, Pb(R_i))$ gave the value for the global minimum, and thus, contained the ROI of the iris, it became

$$\text{ROI} = \arg \min_{R_0 < R_i < R_n} \left(Pb(R_{i+1}) - 2Pb(R_i) + Pb(R_{i-1}) > 0 \right) \tag{6}$$

Measurement

The Figure of Merit (FOM) provided by [16] was used, which is

$$\text{FOM} = \frac{1}{\max(N_1, N_T)} \sum_{i=1}^{N_T} \frac{1}{1 + \alpha d_i^2} \tag{7}$$

where N_1 and N_T refer to the number of ideal and actual edge points, respectively, while, d_i is the pixel Euclidean distance of the *i*th edge detected, and α is the scaling constant selected to be $\alpha = \frac{1}{9}$ and which is used for penalising the displaced edges. The larger FOM value (value between 0 and 1) indicated better performance in the resultant images.

EXPERIMENT AND RESULTS

Eye images contain six regions, like the pupil, iris, sclera, eyelids, eyelashes and the skin. These regions are different from each other, based on their physical, medical and grey level characteristics [17]. Therefore, in this experiment, a histogram of grey level values was used as the feature descriptor, and all the attributes were normalised into the interval (-1,1) to avoid numerical difficulties in the calculation and to minimise the gap between the largest and smallest values [18].

In order to ensure that the suggested method in this study was suitable for iris images, the CASIA V2, which contains a dataset of ideal iris images and the UBIRIS2, which contains a dataset of non-ideal iris images, were selected. The datasets were divided into two parts for use in the training and testing phases. The ROI is an area that is graphically selected from a window displaying an image that contains the information that will be used for a particular purpose. Figure 5 highlights the ROI images that were selected.

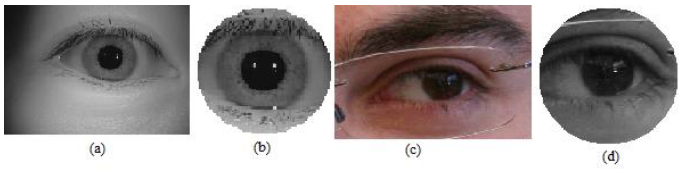

FIG. 5 An example of an original image and the ROI image. (a) Original ideal image from the CASIA V2. (b) ROI image extracted from (a). (c) Original non-ideal image from UBIRIS2. (d) ROI image extracted from (c).

In the training phase, the SVM classifier [19] was used to learn and classify the ROIs of the image. In order to build a model for the training phase of every dataset, data on 50% of the positive samples and 50% of the negative samples were used, as shown in

Figure 6. The positive samples contained the ROI images and the negative samples were circles with reduced or excessively extracted iris images.

(a) (b

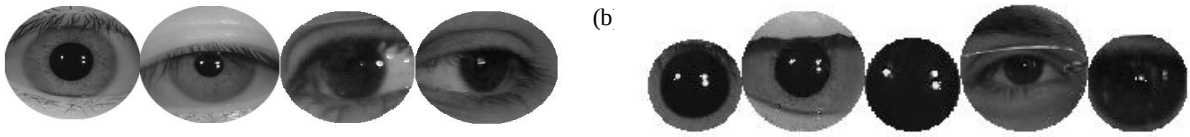

FIG. 6 Examples of (a) positive and (b) negative samples

In the testing phase, the pupil region was detected and extracted, followed by the region growing until the values of $Pb(R_i)$, $Pb(R_{i+1})$ and $Pb(R_{i-1})$ complied with the conditions in Equation (6), whereby that region was selected as the ROI image.

In the experiment, this study used the ideal and non-ideal iris images to obtain the ROI images of the iris in the CASIA V2 and UBIRIS datasets. The results of the effect of the ROI obtained from the adaptive method by [13] are shown in Table 1.

TABLE .1. Results of the effect of the ROI obtained from the adaptive method by [13].

	Without ROI	With ROI
CASIA	0.319678514	0.63930839
UBIRIS	0.206900134	0.579333475

CONCLUSION AND DISCUSSION

The SVM results showed that there was one particular graph pattern, which was that of the graph minimum. The findings indicated that the ROI of the iris was located in the global minimum value of the *Pb* for each dataset that was used. The use of the adaptive method by [13] proved that the utilisation of the proposed method provided an accurate localised iris image that was robust for ideal and non-ideal images. Consequently, the extracted iris region was ready for use in the next stage.

ACKNOWLEDGMENTS

The deepest gratitude and thanks to Universiti Teknikal Malaysia Melaka (UTeM) in supporting this research PJP/2018/FTMK(2B)/S01629.

REFERENCES

[1] Feng, H., & Wah, C. C. (2003). Online signature verification using a new extreme points warping technique. *Pattern Recognition Letters*, *24*(16), 2943–2951. https://doi.org/10.1016/S0167-8655(03)00155-7

[2] Gupta, G. K., & Joyce, R. C. (2007). Using position extrema points to capture shape in on-line handwritten signature verification. *Pattern Recognition*, *40*(10), 2811–2817. https://doi.org/10.1016/j.patcog.2007.01.014

[3] Lu, Y., & Lu, R. (2018). Fast Bi-dimensional empirical mode decomposition as an image enhancement technique for fruit defect detection. *Computers and Electronics in Agriculture*, *152*(June), 314–323. https://doi.org/10.1016/j.compag.2018.07.025

[4] Usman, M., & Usman, M. (2018). Spatial frequency based video stream analysis for object classification and recognition in clouds Spatial Frequency based Video Stream Analysis for Object Classification and Recognition in Clouds

[5] Yang, M. D., Huang, K. S., Yang, Y. F., Lu, L. Y., Feng, Z. Y., & Tsai, H. P. (2016). Hyperspectral Image Classification Using Fast and Adaptive Bidimensional Empirical Mode Decomposition With Minimum Noise Fraction. *IEEE Geoscience and Remote Sensing Letters*, *PP*(99), 1–5. https://doi.org/10.1109/LGRS.2016.2618930

[6] Abiyev, R. H., & Altunkaya, K. (2009). Neural network based biometric personal identification with fast iris segmentation. *International Journal of Control, Automation and Systems*, *7*(1), 17–23. https://doi.org/10.1007/s12555-009-0103-1

[7] Jayalakshmi, S., & Sundaresan, M. (2013). A survey on Iris Segmentation methods. In *2013 International Conference on Pattern Recognition, Informatics and Mobile Engineering* (pp. 418–423). Ieee. https://doi.org/10.1109/ICPRIME.2013.6496513

[8] Negin, M., Chmielewski, T. a., Salganicoff, M., Camus, T. a., Cahn Von Seelen, U. M., Venetianer, P. L., & Zhang, G. G. (2000). Iris biometric system for public and personal use. *Computer*, *33*(2), 70–75. https://doi.org/10.1109/2.820042

[9] Lodin, A., & Demea, S. (2009). Design of an iris-based medical diagnosis system. *2009 International Symposium on Signals, Circuits and Systems, ISSCS 2009*, 3–6. https://doi.org/10.1109/ISSCS.2009.5206187

[10] Ma, L., Tan, T., Wang, Y., & Zhang, D. (2003). Personal identification based on iris texture analysis. *Pattern Analysis and Machine Intelligence, IEEE Transactions On*, *25*(12), 1519–1533. https://doi.org/10.1109/TPAMI.2003.1251145

[11] Sankowski, W., Grabowski, K., Napieralska, M., Zubert, M., & Napieralski, A. (2010). Reliable algorithm for iris segmentation in eye image. *Image and Vision Computing*, *28*(2), 231–237. https://doi.org/10.1016/j.imavis.2009.05.014

[12] Li, Y., Li, W., & Ma, Y. (2012). Accurate iris location based on region of interest. *Proceedings - 2012 International Conference on Biomedical Engineering and Biotechnology, ICBEB 2012*, 704–707. https://doi.org/10.1109/iCBEB.2012.47

[13] Othman, Z., & Abdullah, A. (2018). Adaptive Threshold and Piecewise Fitting for Iris Localisation. *Journal of Telecommunication, Electronic and Computer Engineering (JTEC)*, *10*(2–7), 153–158

[14] Chapra, S. C., & Canale, R. P. (2005). *Numerical methods for engineers* (Vol. 5th). https://doi.org/10.1016/0378-4754(91)90127-O

[15] Strang, G. (1991). *CALCULUS*. Wellesley: Wellesley Cambridge Press

[16] Abdou, I. E., & Pratt, W. K. (1979). Quantitative Design and Evaluation of Enhancement/Thresholding Edge Detectors. *Proc IEEE*, *67*(5), 753–763. https://doi.org/10.1109/PROC.1979.11325

[17] Ibrahim, M. T., Khan, T. M., Khan, S. a., Khan, M. A., & Guan, L. (2012). Iris localization using local histogram and other image statistics. *Optics and Lasers in Engineering*, *50*(5), 645–654. https://doi.org/10.1016/j.optlaseng.2011.11.008

[18] Abdullah, A., Veltkamp, R. C., & Wiering, M. a. (2009). Spatial pyramids and two-layer stacking SVM classifiers for image categorization: A comparative study. *Proceedings of the International Joint Conference on Neural Networks*, 5–12. https://doi.org/10.1109/IJCNN.2009.5178743

[19] Cortes, C., & Vapnik, V. (1995). Support-vector networks. *Machine Learning*, *20*(3), 273–297. https://doi.org/10.1007/BF00994018